Sensitivity of Northern Hemisphere Cyclone Detection and Tracking Results to Fine Spatial and Temporal Resolution Using ERA5🔗

ALEX D. CRAWFORD,[a,b] ERIKA A. P. SCHREIBER,[c,d] NATHAN SOMMER,[e] MARK C. SERREZE,[c]
JULIENNE C. STROEVE,[a] AND DAVID G. BARBER[a]

[a] Centre for Earth Observation Science, University of Manitoba, Winnipeg, Manitoba, Canada
[b] Department of Earth Sciences, College of Wooster, Wooster, Ohio
[c] National Snow and Ice Data Center, Cooperative Institute for Research in Environmental Science,
University of Colorado Boulder, Boulder, Colorado
[d] UNAVCO, Boulder, Colorado
[e] Department of Mathematical and Computational Sciences, College of Wooster, Wooster, Ohio

ABSTRACT: Lagrangian detection and tracking algorithms are frequently used to study the development, distribution, and trends of extratropical cyclones. Past research shows that results from these algorithms are sensitive to both spatial and temporal resolutions of the gridded input fields, with coarser resolutions typically underestimating cyclone frequency by failing to capture weak, small, and short-lived systems. The fifth-generation atmospheric reanalysis from the European Centre for Medium-Range Weather Forecasts (ERA5) offers finer resolution, and, therefore, more precise information regarding storm locations and development than previous global reanalyses. However, our sensitivity tests show that using ERA5 sea level pressure fields at their finest-possible resolution does not necessarily lead to better cyclone detection and tracking. If a common number of nearest neighbors is used when detecting minima in sea level pressure (like past studies), finer spatial resolution leads to noisier fields that unrealistically break up multicenter cyclones. Using a common search distance instead (with more neighbors at finer resolution) resolves the issue without smoothing inputs. Doing this also makes cyclone frequency, life span, and average depth insensitive to refining spatial resolution beyond 100 km. Results using 6- and 3-h temporal resolutions have only minor differences, but using 1-h temporal resolution with a maximum allowed propagation speed of 150 km h^{-1} leads to unrealistic track splitting. This can be counteracted by increasing the maximum propagation speed, but modest sensitivity to temporal resolution persists for several cyclone characteristics. Therefore, we recommend caution if applying existing algorithms to temporal resolutions finer than 3 h and careful evaluation of algorithm settings.

SIGNIFICANCE STATEMENT: Many researchers use computer algorithms that automate detection of extratropical storms and then track those storms through time to better understand how they develop, where they impact people, and how they are changing as the world warms. Conventional wisdom is that using finer spatial and temporal resolutions as inputs to these algorithms improves results by capturing more storms more accurately. However, we find that storm frequency is more sensitive to algorithm settings than to spatial resolution. Making temporal resolution 1-hourly instead of 3-hourly or 6-hourly incorrectly breaks up the tracks of some storms into several smaller pieces. In either case, our datasets have improved enough so that a finer resolution is no longer always better.

KEYWORDS: Atmosphere; Extratropical cyclones; Storm tracks; Sensitivity studies

---

1. Introduction

Lagrangian detection and tracking algorithms are common tools to assess the frequency and development of extratropical cyclones (e.g., Rudeva and Gulev 2007; Allen et al. 2010; Crawford and Serreze 2016), the spatial and seasonal distributions of their tracks (e.g., Murray and Simmonds 1991; Serreze 1995; Hodges et al. 2003; Wernli and Schwierz 2006;

Pinto et al. 2016), and their responses to a changing climate (e.g., Ulbrich et al. 2008; Day et al. 2017; Raible et al. 2018). These algorithms have also been used to assess extreme events (e.g., Simmonds and Rudeva 2014; Reale et al. 2019) and extratropical cyclone impacts on the surface, such as freshwater fluxes (Finnis et al. 2007; Stroeve et al. 2011; Papritz et al. 2014), high surface winds (Inatsu 2009; Hewson and Neu 2015), ocean swell (Hell et al. 2020), rain-on-snow (Crawford et al. 2020), and the melting and breakup of sea ice (Rae et al. 2017; Schreiber and Serreze 2020). These algorithms involve a diversity of input datasets, input variables, preprocessing, and detection and tracking settings, which all influence the tracking results (e.g., Blender and Schubert 2000; Raible et al. 2008; Neu et al. 2013; Vessey et al. 2020).

Results of cyclone detection and tracking are often described as "improved" when using data with finer spatial

---

resolution (e.g., 1° vs 2° or 6 vs 12 h; Blender and Schubert 2000; Pinto et al. 2005; Jung et al. 2006). For example, weak and open cyclones go undetected when using gridded input fields at coarser spatial resolution (Blender and Schubert 2000; Pinto et al. 2005; Jung et al. 2006; Di Luca et al. 2015; Wang et al. 2016). This occurs both as a direct result of finer spatial scale (e.g., Blender and Schubert 2000), but also indirectly from better physical representation in finer-scale models (e.g., Jung et al. 2006; Wang et al. 2016).

However, Rohrer et al. (2020) conclude differently. Only one of the algorithms they examined (Blender et al. 1997) resulted in more storms at a T639 resolution (about 31 km at the equator) compared to a resolution of 1° latitude or T63 (about 110 or 210 km at the equator, respectively). The other algorithm (Wernli and Schwierz 2006) detected fewer storms at a finer resolution because it merges any cyclone centers within 1000 km of each other (Rohrer et al. 2020). Some algorithms use spectral filtering to smooth the input data to a standard resolution, such as T42 (about 310 km at the equator) as used by Hoskins and Hodges (2002) and Côté et al. (2015). Merging or smoothing techniques reduce sensitivity to spatial resolution but underrepresent smaller systems and secondary cyclogenesis (Rohrer et al. 2020).

Higher temporal resolution can also lead to higher cyclone counts. Low temporal resolution (e.g., 12 h) can result in late identification of cyclogenesis (Blender and Schubert 2000), truncating tracks so that systems no longer surpass minimum life-span or track-length thresholds (Rudeva et al. 2014). Tracking is also less certain at coarser temporal resolutions, especially for fast-moving storms (Rudeva et al. 2014). Pinto et al. (2005) found that going from 12- to 6-h resolution increased track counts in part because it reduced the number of storms being split during the point of maximum propagation.

The coarsest resolution used in each of these sensitivity studies was 200 km (or coarser), and at least two sensitivity studies have considered spatial resolutions finer than 100 km (Di Luca et al. 2015; Rohrer et al. 2020). This spans the variety of spatial resolutions used in cyclone detection and tracking applications [e.g., 30 km in Tilinina et al. (2014), 50 km in Wang et al. (2016), 100 km in Crawford and Serreze (2017), 1.125° in Wernli and Schwierz (2006), 1.5° in Neu et al. (2013), 1.875° in Hodges et al. (2011), or 2.5° in Simmonds et al. (2008)]. Most cyclone tracking studies use input fields with a temporal resolution of 6 h or coarser (e.g., Neu et al. 2013; Wang et al. 2016; Sprenger et al. 2017; Rohrer et al. 2018; Vessey et al. 2020), although some have used 3-h or finer resolution (e.g., Tilinina et al. 2014; Crawford et al. 2020; Hell et al. 2020). Often, the same detection and tracking algorithm has been applied to datasets with different spatial or temporal resolutions using identical settings (such as thresholds for maximum propagation speed or minimum sea level pressure gradients for cyclones) for all resolutions (e.g., Blender and Schubert 2000; Pinto et al. 2005). Rohrer et al. (2020) cautioned that because results from these algorithms are sensitive to spatial resolution, different input datasets likely require different input settings. However, few studies have addressed how algorithm settings interact with different spatial and temporal resolutions.

The availability of finer-resolution datasets such as the fifth generation of the European Centre of Medium-Range Weather Forecasts (ECMWF) global atmospheric reanalysis (ERA5) with T639 and 1-h resolution (Hersbach et al. 2020), provides the opportunity to detect cyclones with greater precision and extract richer information regarding their development, intensity, size, tracks, and spatial frequency. However, running detection and tracking algorithms at finer resolution has a computational cost. Additionally, just as pre-existing algorithms may need to be modified to adequately handle data with finer spatial resolution (Rohrer et al. 2020), they may also need modification to handle data with finer temporal resolution.

Here we examine the sensitivity of cyclone detection and tracking in ERA5 for the Northern Hemisphere using a single algorithm [introduced by Crawford and Serreze (2016)] to finer spatial and temporal resolutions than typically used, comparing 200-, 100-, 50-, and 25-km spatial resolutions and 6-, 3-, and 1-h temporal resolutions. Our research questions include:

1) Does further refinement of resolution to 25 km and 1 h enhance the ability of algorithms to capture small/weak and fast-moving systems, respectively?

2) Do any problems arise when applying an algorithm built for 200-/100-km and 6-/3-h data to finer resolution?

3) How do common algorithm settings like the number of neighbors used when detecting local minima or the maximum propagation speed allowed for continuing cyclone tracks impact the sensitivity of results to data resolution?

2. Data and methods

a. ERA5 data

ERA5 (Hersbach et al. 2018) has the finest resolution of any global atmospheric reanalysis: 1-h temporal resolution and T639 spatial resolution (Hersbach et al. 2020). ERA5 also improves on its predecessor (ERA-Interim) by using a hybrid incremental 4D-Var system and additional data sources for assimilation. ERA5 includes a weakly coupled land data assimilation system, optimal interpolation for ocean wave heights, and uncertainty estimation (Hersbach et al. 2020). Hourly mean sea level pressure (SLP) fields for the Northern Hemisphere were retrieved for 1979–2019 at a $0.25 \times 0.25°$ spatial resolution and regridded to a north-polar Lambert azimuthal equal-area grid (Brodzik et al. 2012) with resolutions of 200 km (90 cells $\times$ 90 cells), 100 km (180 cells $\times$ 180 cells), 50 km (360 cells $\times$ 360 cells), and 25 km (720 cells $\times$ 720 cells). Consistent with findings of Rohrer et al. (2018), results in this study are robust to interpolation method (Fig. S1 in the online supplemental material). Because of uncertainties arising from the extrapolation of surface pressure from high elevation to sea level, grid cells at elevations exceeding 1500 m [based on ETOPO1; NOAA National Geophysical Data Center (2009)] were masked. ETOPO1 leads to a more conservative mask than using ERA5's orography.

b. Algorithm description

The cyclone detection and tracking algorithm used here was introduced by Crawford and Serreze (2016) and builds on the

TABLE 1. Total search area for detecting if a grid cell is a local SLP minimum based on spatial resolution X and search distance (D). The total search area is calculated as $(2D + X)^2$. Two methods for determining the search distance are used: 24 nearest neighbors for all spatial resolutions or a common 200-km search distance for all spatial resolutions.

		Spatial resolution			
		200 km	100 km	50 km	25 km
24 nearest neighbors (5 × 5 kernel)	Total cells	5 × 5	5 × 5	5 × 5	5 × 5
	Search distance (km)	400	200	100	50
	Search area (km)	1000 × 1000	500 × 500	250 × 250	125 × 125
200-km search distance	Total cells	3 × 3	5 × 5	9 × 9	17 × 17
	Search distance (km)	200	200	200	200
	Search area (km)	600 × 600	500 × 500	450 × 450	425 × 425

algorithm originally designed by Serreze (1995). Spatial distributions of cyclone frequency in both winter and summer compare well to results from algorithms surveyed by Neu et al. (2013) when run on ERA-Interim data at 100-km spatial resolution and 6-h temporal resolution [see supplemental material in Crawford and Serreze (2016)]. However, its detection of more cyclones in winter than in summer for the Northern Hemisphere matches results of relative-vorticity-based algorithms, unlike most SLP-based algorithms. It has also been applied to NASA's Modern-Era Retrospective Analysis for Research and Applications (MERRA; Koyama et al. 2017), MERRA2 (Crawford et al. 2020), ERA5 (Hell et al. 2020), and the Community Earth System Model (Crawford and Serreze 2017) with a range of resolutions from 1 to 6 h and 50 to 250 km. Since each of these projects focused on different input datasets and/or regions of the globe, no formal study has yet been conducted on the sensitivity of this algorithm to resolution.

Cyclone detection begins with the detection of local SLP minima. The definition of "local" is 24 nearest neighbors (i.e., a 5 × 5 detection kernel) as our reference case for this study, following Crawford et al. (2020). Many past studies (e.g., Blender and Schubert 2000; Wernli and Schwierz 2006; Akperov et al. 2019) used eight nearest neighbors (i.e., a 3 × 3 kernel). SLP minima are discarded if 1) more than 40% of neighbors are masked for elevation or 2) the SLP difference between the minimum and the grid cells in a radius of 1000 km around it is less than 7.5 hPa. This is stricter than several studies (e.g., Pinto et al. 2005; Wernli and Schwierz 2006; Di Luca et al. 2015) but the same as Hanley and Caballero (2012).

Rather than assume that any cyclone centers within 1000 or 1200 km are part of the same system (e.g., Zhang et al. 2004; one algorithm in Rohrer et al. 2020), this algorithm explicitly detects the presence of multicenter cyclones (MCCs) at the same time as calculating cyclone area, following Hanley and Caballero (2012). Similar to other algorithms (e.g., Wernli and Schwierz 2006; Hanley and Caballero 2012; Akperov et al. 2015), cyclone area is defined via the outermost closed isobar, meaning the isobar with the highest SLP that encloses the cyclone center of interest but no centers from other cyclones and no SLP maxima. Secondary centers are assigned to a cyclone if 1) they are within 1200 km and 2) doing so at least doubles the cyclone area. Otherwise, the centers in question are treated as separate cyclones.

The location ($\mathbf{x}_i$) of each cyclone center in time t is predicted based on past propagation as $\mathbf{x}_i^*(t) = \mathbf{x}_i(t - 1) + 0.75[\mathbf{x}_i(t - 1) - \mathbf{x}_i(t - 2)]$. The factor of 0.75 accounts for deceleration common to aging storms (Hanley and Caballero 2012). Each cyclone track is extended to the nearest cyclone center in time t to $\mathbf{x}_i^*(t)$ that is also within $t_{res}^*(150 \text{ km h}^{-1})$ of $\mathbf{x}_i(t - 1)$, where t_{res} is the temporal resolution in hours. If no cyclone center in time t satisfies these criteria, cyclolysis is assumed. If multiple centers meet the criteria and are not assigned to another track, cyclone splitting occurs. If two tracks from $t - 1$ are assigned to the same center in time t, cyclone merging occurs. For merges and splits, the nearest neighbor is given preference for track continuation, with the deeper cyclone selected if distance is the same. Cyclogenesis occurs if a center in time t is not within $t_{res}^*(150 \text{ km h}^{-1})$ of any preexisting track.

c. Resolution and setting experiments

Our comparisons of cyclone detection were performed at four spatial resolutions: 200, 100, 50, and 25 km (Table 1). Additionally, based on the resulting differences in cyclone center detection, two methods were examined for determining the number of nearest neighbors to consider when detecting local SLP minima: 1) using a common number of nearest neighbors, as in past sensitivity studies (e.g., Blender and Schubert 2000; Jung et al. 2006) and 2) using a common search distance of 200 km, which leads to a variable number of neighbors.

These two methods yield no differences at 100-km spatial resolution, for which they both yield a search area of 5 cells × 5 cells (500 km × 500 km; Fig. S2). Using a common number of neighbors allows cyclone centers to exist closer together as spatial resolution increases, whereas the 200-km search distance forces all cyclone centers to be over 200 km apart regardless of spatial resolution.

Cyclone tracking was performed at three temporal resolutions: 6, 3, and 1 h (Table 2). Additionally, based on the resulting differences in cyclone tracking, two different maximum allowed propagation speeds (V_{max}) for cyclones were considered: 1) a constant value of $V_{max} = 150 \text{ km h}^{-1}$ and 2) a dynamic value scaling from 125 to 300 km h^{-1} from 6- to 1-h resolution. This experiment is merely meant to illustrate sensitivity, so the exact values are not necessarily ideal. The general effect is to allow faster propagation of tracks at a finer temporal resolution, and the reasoning for this experiment will

TABLE 2. Temporal resolution and maximum propagation speed setting for tracking cyclone centers.

	Temporal resolution					
	6 h		3 h		1 h	
	Speed (km h^{-1})	Distance (km)	Speed (km h^{-1})	Distance (km)	Speed (km h^{-1})	Distance (km)
Constant max propagation	150	900	150	450	150	150
Dynamic max propagation	125	750	192	564	300	300

be described in section 3b. Both modifications represent a change to input settings rather than a fundamental change to the cyclone detection and tracking algorithm. Finally, note that storms are not tracked at a 200-km/1-h resolution with a maximum propagation speed of 150 km h^{-1} because the minimum nonstationary propagation possible would be 200 km over 1 h.

d. Comparison methods

Results using different spatial resolutions and search distances are assessed in several ways. The number of SLP minima, centers, and cyclones are counted for each SLP field, as are the average ratio of centers to cyclones and the average area of cyclones in each field. Comparing centers and cyclones helps determine how the detection of MCCs interacts with spatial resolution and search distance.

Before direct comparison, cyclone tracks are subset to only those that 1) have a life span of at least 24 h, 2) have a track length of at least 1000 km, and 3) are observed at least once over an elevation less than 500 m. This helps filter out spurious storm systems. Cyclone tracks are compared in three ways. First, the average number of tracks per year, and the percentage of tracks that are MCCs or experience merges and/or splits are tabulated, as are average life span, track length, propagation speed, area, central pressure, and depth. (Depth is the pressure of the outermost isobar minus the central pressure.) Results from each experiment are compared graphically and with single-factor ANOVA followed by Games–Howell tests for pairwise comparisons. Second, track occurrence, genesis events, and lysis events are all mapped to a common 200-km and 1-h resolution (Zolina and Gulev 2002) and smoothed (Crawford and Serreze 2016). Track density is defined as the number of tracks that pass through an 800 km × 800 km area centered on each grid cell for a given period. Event density is the number of events (genesis or lysis) that occur within an 800 km × 800 km area for a given period.

Third, a track-matching scheme based on Hodges et al. (2003) is used to see how well the tracks in two experiments (e.g., different temporal resolutions or different settings) match across time and space. For each track in experiment 1, the time overlap with all experiment 2 tracks is assessed first. Assume that n_1 and n_2 are the number of time observations in experiment 1 and experiment 2, respectively, and n_m is the number of observations that share the same time. A potential match exists if $2n_m/(n_1 + n_2) \geq 0.60$, meaning both tracks exist in at least 60% of their combined observation times. For comparing experiments with different temporal resolutions, the least common multiple of their resolutions is used (i.e., only observations at times 0000, 0600, 1200, and 1800 UTC are used

when comparing 1- and 6-h experiments). For any pair of tracks meeting the time criterion, the average distance between the tracks is calculated for all shared observation times. If the average separation is no more than 500 km, the tracks are matched. If multiple tracks in experiment 2 fit these criteria, the experiment 2 track with the smallest average separation is kept as the best match for the given experiment 1 track.

3. Results

a. Sensitivity of cyclone detection to spatial resolution

The number of SLP minima, cyclone centers, and cyclone systems all have a strong dependence on spatial resolution when using a common number of nearest neighbors to identify SLP minima (Fig. 1). Over 1900 SLP minima are identified per SLP field using a 25-km resolution, which is almost 10 times greater than for a 100-km resolution. Over 4 times as many minima are identified at 100- than at 200-km resolution. These differences are slightly greater in winter than summer (not shown). The intensity criterion [7.5 hPa (1000 km)$^{-1}$] removes most of the additional SLP minima at finer resolution, so only twice as many cyclones (34.7 vs 17.6) are identified for 25-km SLP fields compared to 100-km SLP fields. The number of cyclones in 200-km fields is even lower, at 13.7 cyclones per field. Although almost all past studies have found that more cyclones are identified at finer spatial resolution, this does not necessarily mean finer spatial resolution is more accurate. Inputting finer resolution data to the algorithm increases the likelihood of identifying smaller systems but risks incorrectly dividing a multicenter cyclone (MCC) into several different cyclones. Therefore, it is important to assess whether an increase in cyclone counts is the result of 1) identifying smaller/weaker cyclones that are truly distinct systems or 2) identifying more centers in a single large MCC and incorrectly breaking it up.

These two possibilities can be assessed in several ways. First, examining example SLP fields helps to illustrate that, when using a common number of nearest neighbors, the additional cyclone centers detected at finer resolutions are mostly clustered within the cyclone areas defined at coarser resolution (Figs. 2a–d). For example, the cyclones located over Baffin Bay and Mongolia at 0000 UTC 26 October 2012 change from having two and three centers, respectively, at 100-km resolution to 5 and 11, respectively, at 25-km resolution. However, the algorithm does not maintain these systems as MCCs; rather, it unrealistically splits them into multiple distinct systems. Using a coarser 200-km resolution, these two storms have roughly the same area as at 100-km, but they are now identified as single-center cyclones.
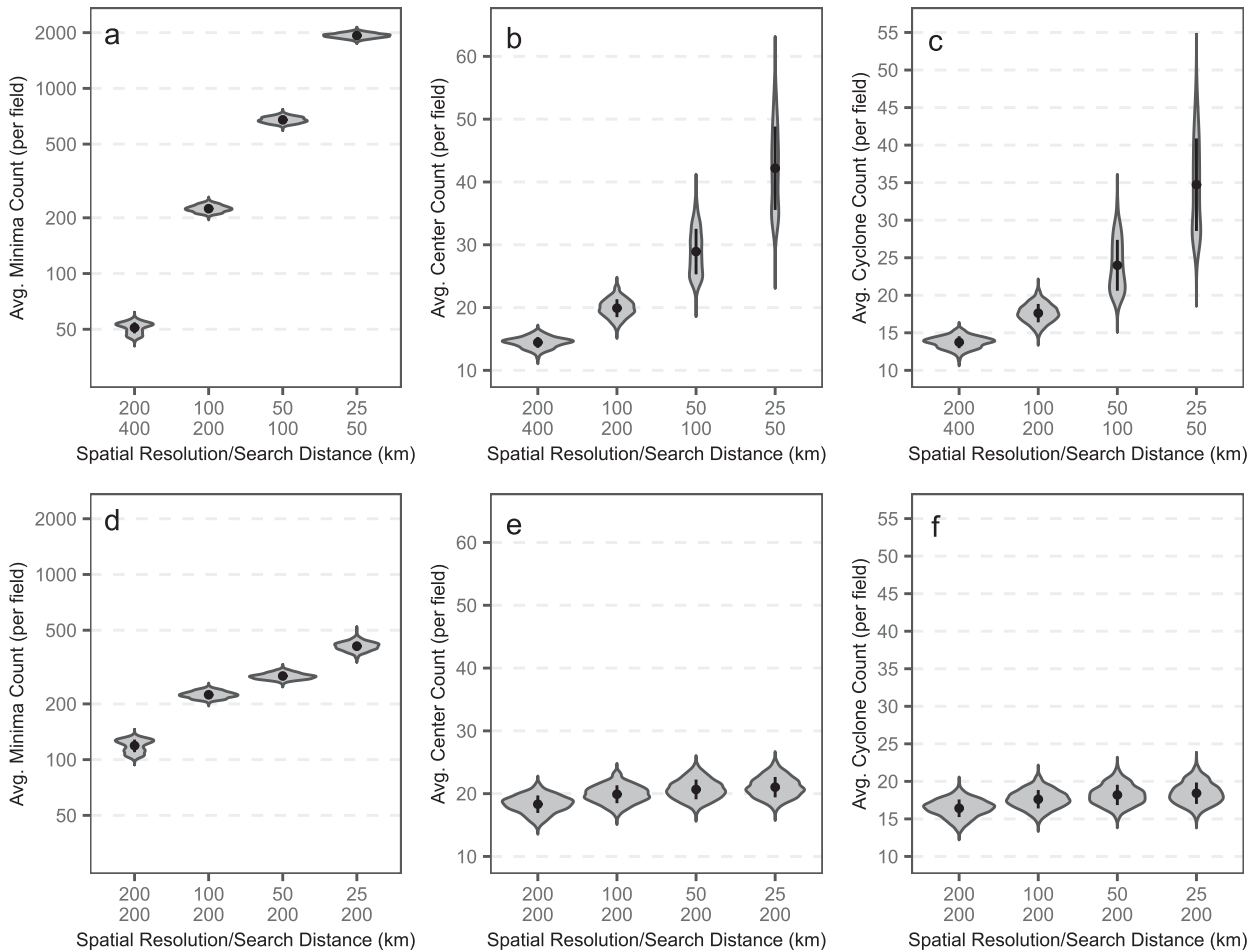
FIG. 1. Average number of (a),(d) SLP minima; (b),(e) cyclone centers; and (c),(f) cyclone systems per 6-h SLP field for different combinations of spatial resolution and search distance. All means are significantly different from each other ($p < 0.05$) except for the cyclone count between 50 and 25 km in (f).

Similar results emerge for other examples (Figs. S3–S5), and unrealistic breakups are also reflected in aggregated statistics of SLP fields (Figs. 3a–d). Although cyclone center density is greater for finer spatial resolutions across the Northern Hemisphere, it is most acute around areas of complex topography, such as Alaska, the margin of Greenland, and Kamchatka. With a 200-km resolution, 24 nearest neighbors cover a 1000 km × 1000 km area, but with a 25-km resolution, 24 nearest neighbors cover only 125 km × 125 km (Fig. S2). As a result, the detection scheme can find cyclone centers much closer to the areas of masked elevation at finer resolution.

Some of the additional centers detected at a finer resolution are incorporated into MCCs. In the aggregate, this is reflected as a higher ratio of centers to cyclones in SLP fields. The ratio increases from about 1.05 to 1.21 when going from 200- to 50-km (or 25-km) spatial resolution (Fig. 4b). However, the total area covered by cyclones drops from 22.7 million km^2 per field at 200-km resolution to under 12.4 million km^2 at 50-km resolution (Fig. 4a). Going even finer, to 25 km, the decline in total area is even greater. Despite the increase in cyclones

detected at finer spatial resolution, the total area influenced by cyclones drops by about 45% from 200- to 50-km resolution (and by 58% going to 25-km resolution). This is surprising. If all additional centers at finer resolution were identified as secondary centers in MCCs, then more centers would be added to the same cyclone area, so the area would stay the same on average. If the additional centers are identified as previously undetected systems, the total area should increase on average. In neither case would a decrease in total area be expected.

Taken together, these results indicate that refining spatial resolution to 25 km while using a common 24 nearest neighbors for detecting SLP minima unrealistically breaks up large, complex systems into multiple distinct storms, overwhelming the MCC detection component of the algorithm. This issue could be avoided by only using a coarser resolution, but at the cost of less precision. Therefore, we experiment with using a common search distance for SLP minima detection rather than a common number of nearest neighbors (Fig. S2). This is similar to enforcing a minimum distance between cyclone centers (e.g., one method in Rohrer et al. 2020). The final three violin plots in each graph from Figs. 1 and 4 and the final three
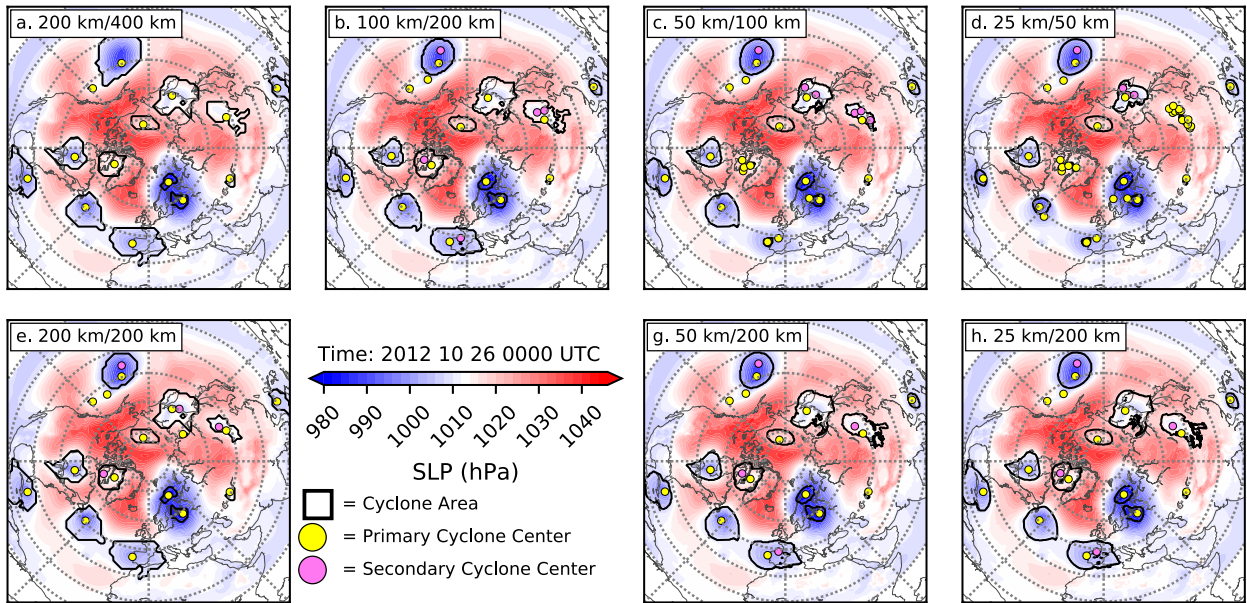
FIG. 2. Example SLP field from 0000 UTC 26 Oct 2012 using five combinations of spatial resolution and search distance. SLP (filled contours) is overlain with cyclone areas (black outlines), the primary cyclone center for each system (yellow dots), and any secondary cyclone centers in MCCs (pink dots).

maps in Fig. 3 use this common 200-km search distance for all resolutions.

With a common search distance, the 25-km resolution yields only about two additional cyclones per SLP field compared to 200-km resolution (18.4 vs 16.4; $p < 0.01$; Fig. 1f). Using 100-km (17.6) and 50-km (18.2) resolutions yield results within

one cyclone/field of the 25-km data. The only significant difference for total area is between 200-km resolution and the others (Fig. 4c). Similarly, the center to cyclone ratios are nearly identical for 100-km (1.13), 50-km (1.14), and 25-km (1.14) resolutions (Fig. 4d). Cyclone center density is generally lower at 200-km than 100-km, especially near the terminus of the
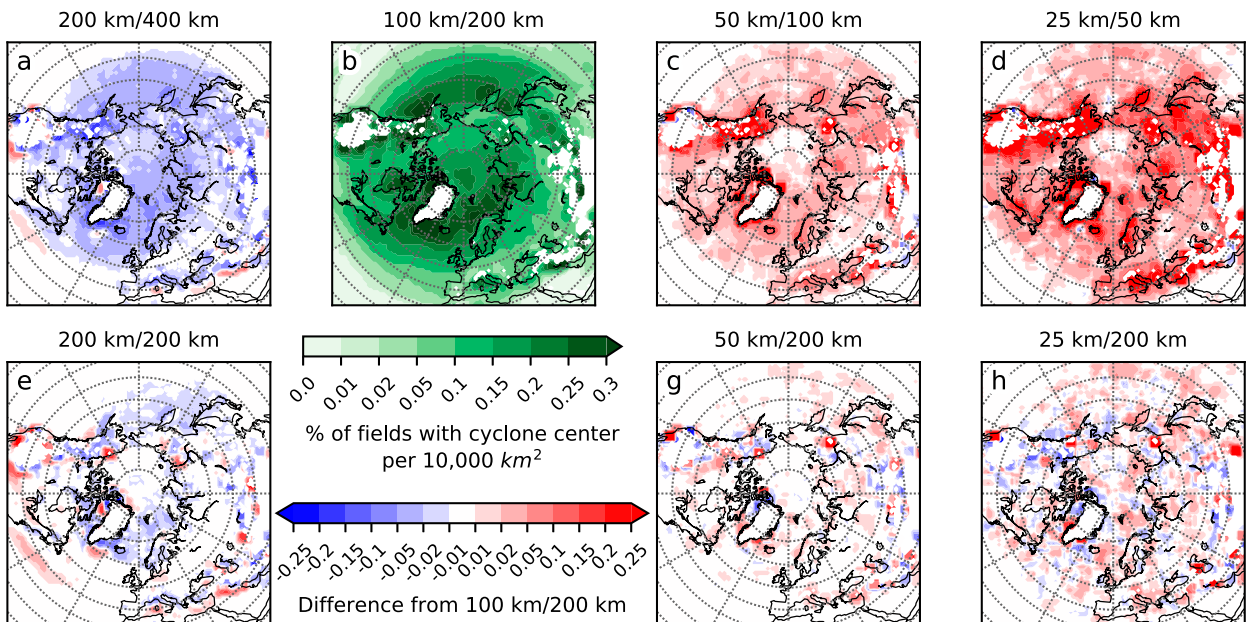

FIG. 3. Spatial distribution of cyclone center density for five combinations of spatial resolution and search distance. Areas over 1500 m elevation are masked. The 100-km-resolution climatology in (b) is subtracted from other climatologies in (a) and (c)–(h). All colored values have a significant difference ($p < 0.05$).
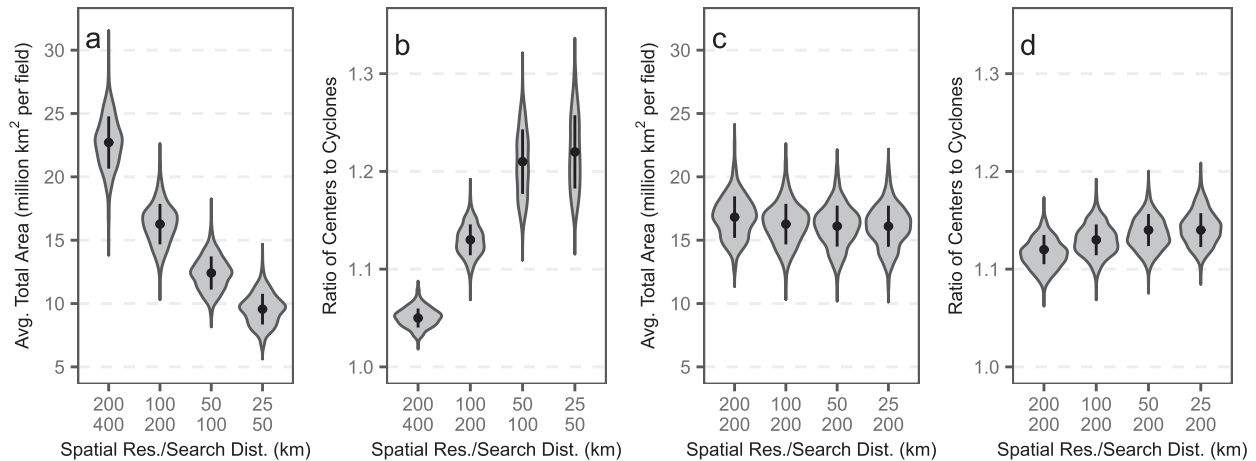
FIG. 4. Violin plots showing distribution of (a),(c) average total cyclone area and (b),(d) ratio of centers to cyclones by 6-h SLP field for different combinations of spatial resolution and search distance. All means are significantly different from each other ($p < 0.05$) in (a), (b), and (d). Only 200-km spatial resolution results are significantly different from the others in (c).

North Atlantic storm track and much of the North Pacific storm track (Fig. 3e). However, 50- and 25-km data show minor and spatially heterogeneous differences from 100-km data (Figs. 3g–h). Therefore, at 100-km or finer spatial resolution, cyclone detection has low sensitivity to spatial resolution if a common search distance is employed. After the tracking stage of the algorithm, aggregate statistics like the average life span and average intensity also show little sensitivity to spatial resolution when using a common search distance for cyclone detection (Figs. S6 and S7).

b. Sensitivity of cyclone tracking to temporal resolution

Past studies have concluded that using finer temporal resolution leads to more accurate tracking because tracking is simpler and less prone to error when the features travel shorter distances between each observation time (Blender and Schubert 2000; Pinto et al. 2005; Rudeva et al. 2014). If storms are assumed to propagate no faster than some maximum propagation speed (e.g., 60, 100, and 150 km h^{-1}; hereafter, V_{max}), the search radius necessary to find the best match for continuing a cyclone track in the next observation time will shrink for finer temporal resolution (Fig. S8). That implies better tracking because, with fewer potential matches for track continuation, the chances of an incorrect match are lower (Pinto et al. 2005). Using a finer temporal resolution should also make genesis and lysis more precise, reducing the chance of late detection or early termination of a track that may force it under the oft-used 24-h minimum life-span threshold (Rudeva et al. 2014).

Based on these factors, going from 6- to 1-h resolution should lead to more storms being detected. However, it is primarily the shorter tracks that are sensitive to late detection or early termination, so the addition of more short-lived tracks at finer resolution may lead to a reduction in average track length and life span. Additionally, since systems with shorter tracks are also often smaller, less intense systems, we expect that the average storm will be weaker at a finer resolution.

Finally, we would expect fewer storm splitting and merging events at a finer resolution because of the smaller search radius during tracking.

However, when examining aggregated cyclone-tracking characteristics for 6-, 3-, and 1-h resolution with constant 50-km spatial resolution (Fig. 5; Fig. S9), not all these expectations are met. At finer temporal resolution, average track length is shorter, but the number of cyclone tracks is also reduced. The percentage of storms that have splits or merges is reduced, which is consistent with expectations, but the average storm is more intense (lower central pressure and greater depth) and larger by about 35% from 6- to 1-h resolution.

Examples of cyclone tracks for specific periods help reveal the cause of this unexpected behavior. Plotting all tracks for storms whose life span intersects the period 1–6 Aug 2012 reveals that many tracks apparent at a 6-h resolution are truncated or split at a 1-h resolution (Figs. 6a–c). Indeed, they are split so often that fewer storm tracks pass the life-span and track length thresholds meant to filter out spurious systems (Figs. 6d–f). Secondary cyclogenesis, defined here as continuation of a track by a secondary center of a multicenter cyclone when the original primary center has dissipated, is also more prevalent at finer temporal resolution, but this does not fully compensate for the reduction in tracks.

Track splitting impacts even the largest and strongest storms, such as the "Great Arctic Cyclone" of August 2012 (Simmonds and Rudeva 2012). At a 6-h resolution, the algorithm used here detects cyclogenesis for this storm at about 61.5°N, 102.0°E at 1800 UTC 2 August 2012 and cyclolysis at 75.7°N, 100.0°W at 0000 UTC 14 August 2012. The algorithm used by Simmonds and Rudeva (2012) explicitly detects open cyclones and identifies the storm existing both earlier on 2 Aug 2012 and later on 14 Aug 2012, but tracks are otherwise identical. Although this storm's track is maintained at 3-h resolution, it is split into five pieces at a 1-h resolution, only one of which lasts at least 24 h and has a length of at least 1000 km.
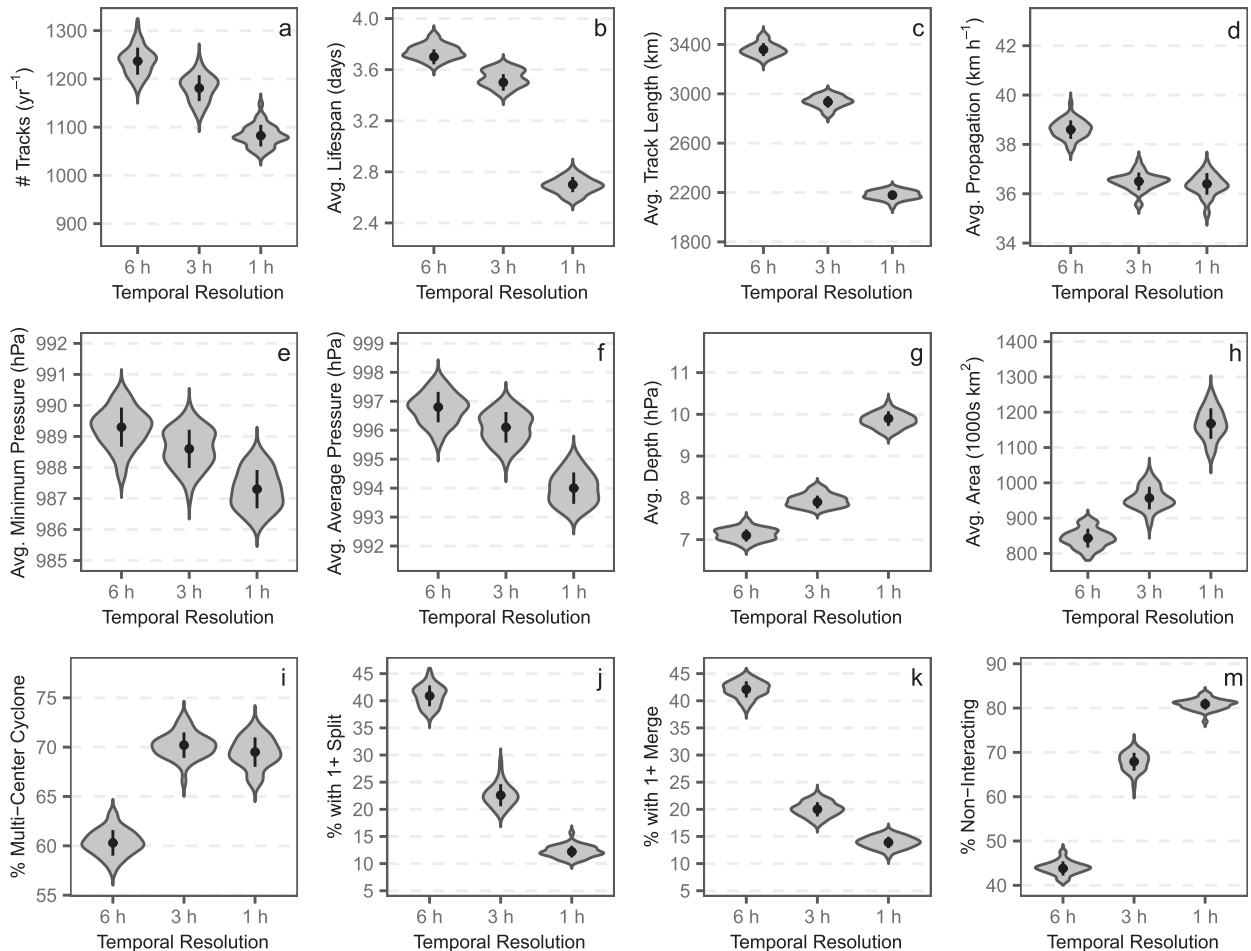
FIG. 5. Violin plots showing the distribution of annual averages of cyclone track statistics for 50-km spatial resolution, 200-km search distance, constant maximum propagation speed, and three temporal resolutions. (d)–(h) Annual averages (1979–2019) are calculated from the track-wise minima/averages of each metric. Dots and lines within each plot represent the mean $\pm$ 1 standard deviation. All means are significantly different from each other ($p < 0.05$) except for comparing 1–3 h in (d) and (i).

This sensitivity to temporal resolution is most acute at a coarser spatial resolution (Figs. S10 and S11). This is likely because at a 100-km spatial resolution, the temporal resolution is too fine for the spatial resolution. A fast-propagating cyclone (e.g., 110 km h^{-1}) could conceivably move from the edge of one grid cell, entirely across another 100-km grid cell, and into a third one in a single time interval, apparently moving 200 km h^{-1}, which is above the V_{max} of 150 km h^{-1}. Alternatively, a cyclone propagating at 30 km h^{-1} may remain in a single grid cell for multiple observations, apparently not moving. This leads to bimodal distributions of propagation speed for storms being tracked at 1-h on a 100-km grid; propagation is most often either 0 km h^{-1} or about 100 km h^{-1} (see the example storm in Fig. 7a). At finer spatial resolution or coarser temporal resolution, storms are capable of propagating across multiple grid cells for one time interval, leading to more unimodal distributions that are less sensitive to temporal resolution.

However, an interaction with spatial resolution cannot entirely explain the discrepancy between finer and coarser temporal resolution (Fig. 5). Even at a 25-km resolution, 1-h

tracking still leads to unrealistic splitting of storms when propagation speeds are greatest (Figs. S12 and S13). The V_{max} of 150 km h^{-1} used in this algorithm is already more generous than the threshold adopted in many other algorithms (Neu et al. 2013), and for a 6- and 3-h resolution it yields reasonable results. Why, then, would it fail at 1-h resolution? One explanation is that the "center" of a cyclone is not necessarily its geometric center, but rather its point of greatest depth (i.e., lowest pressure). As a cyclone develops, the location of its deepest point relative to the system can change. Thus, the propagation of a cyclone center is a combination of the advecting flow and the cyclone's internal development. It is therefore possible that a center can appear to move faster than the system overall when the deepest point changes, introducing error no greater than the storm's diameter (Fig. S14). Storm diameter is not dependent on temporal resolution, but the distance a storm propagates decreases with finer temporal resolution. Therefore, error in propagation speed from internal cyclone development can be a greater percentage of the propagation at finer temporal resolution.
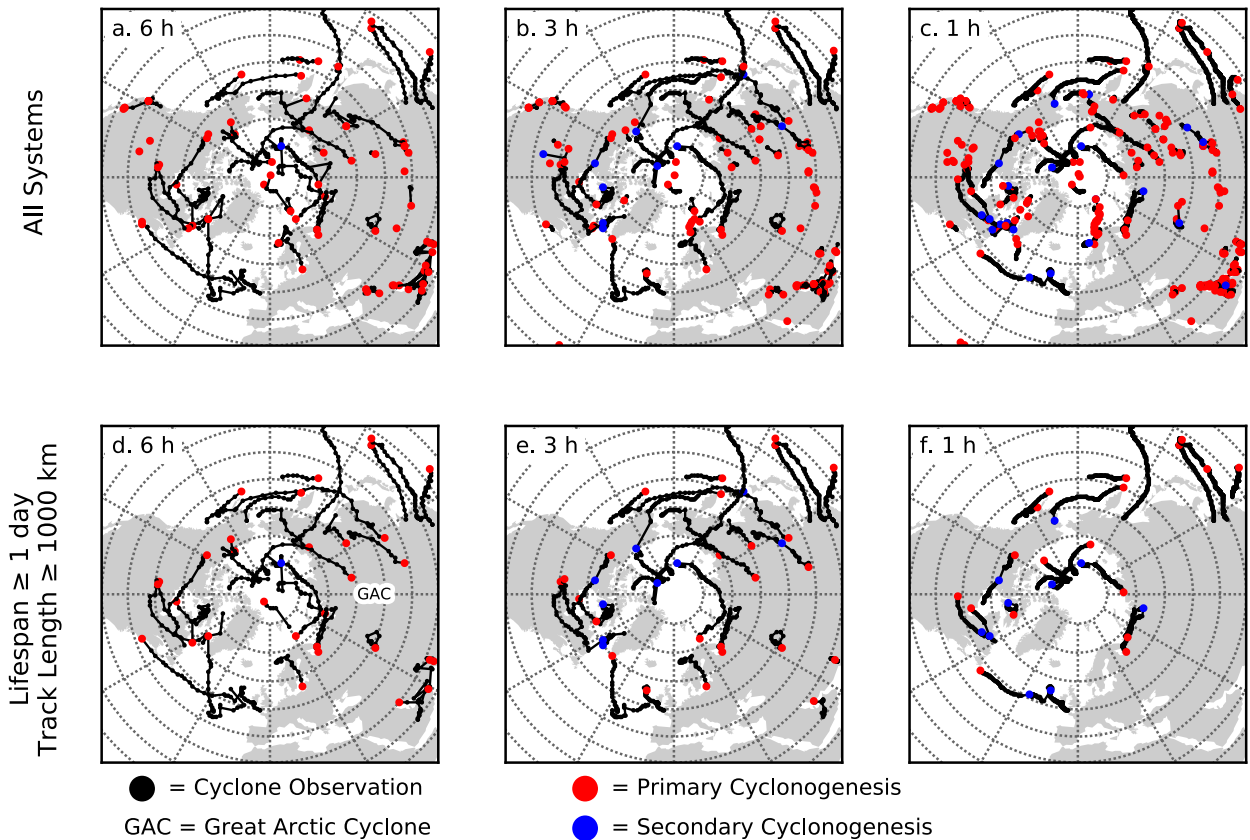
FIG. 6. Example of cyclone tracking for 50-km spatial resolution, 200-km search distance, constant maximum propagation speed, and three temporal resolutions. (a)–(c) All systems active for at least part of the period 1–6 Aug 2012. (d)–(f) For the same period as in (a)–(c), but only those tracks lasting at least 1 day and 1000 km.

One potential solution is to track cyclones as areas rather than as locations of pressure minima [as in Inatsu (2009) or Kew et al. (2010)]. However, that would require a fundamentally new tracking algorithm design. A more modest approach is to change V_{max} based on temporal resolution. Essentially,

the faster V_{max}, the more likely that a cyclone track will be continued for any time interval. For example, using 125 km h^{-1} instead of 150 km h^{-1} eliminates one storm in the period 1–6 Aug 2012 for 6-h data and truncates a few other tracks (Fig. 8a vs 8d). Using 192 km h^{-1} for 3-h data (Fig. 8e) yields results
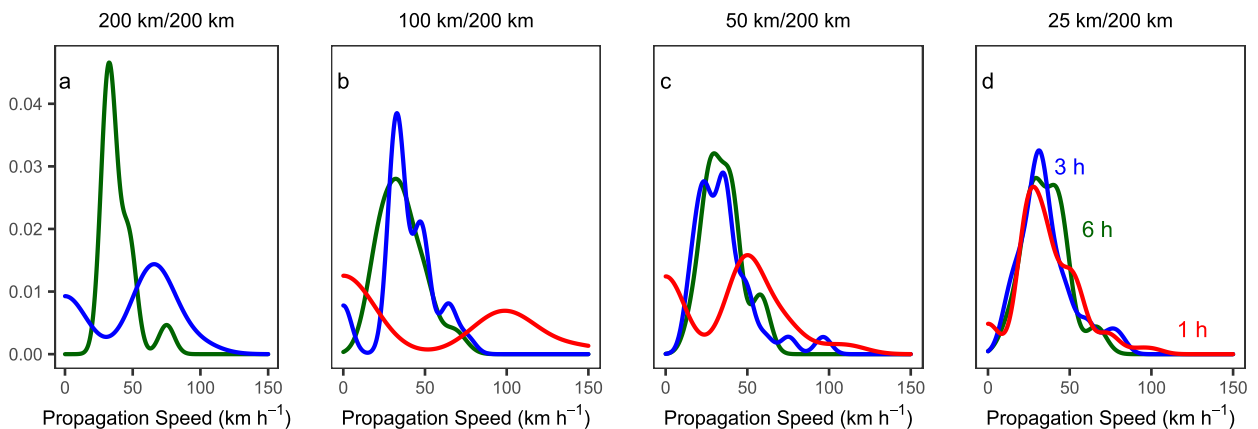

FIG. 7. Density plots of propagation speed for the cyclone tracking from the southern tip of Kamchatka (49.5°N, 156.7°E) to southeast Alaska (60.5°N, 162.7°W) in the first week of August 2012 (see Fig. 6) for 6- (green), 3- (blue), and 1-h (red) temporal resolution and (a) 200-, (b) 100-, (c) 50-, and (d) 25-km spatial resolution. Only the section of the track that can be directly matched in all experiments is included.
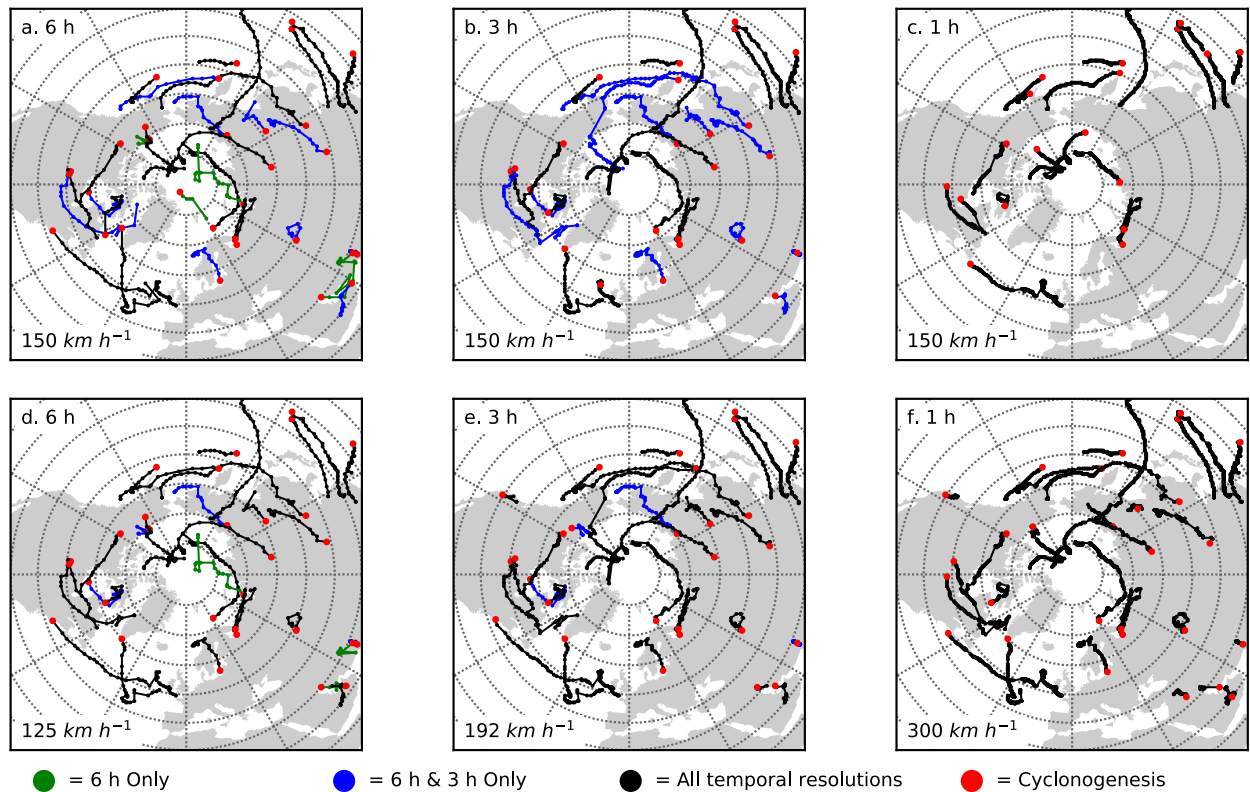
FIG. 8. Example of cyclone tracks for 50-km spatial resolution and 200-km search distance for all storms that last at least 1 day and 1000 km and whose life spans intersect the period 1–6 Aug 2012. Maximum propagation speed is (a)–(c) 150 (d) 125, (e) 192, and (f) 300 km h^{-1} for (left to right) 6-, 3-, and 1-h resolutions, respectively. Red indicates cyclogenesis locations; all other colors indicate in which experiments the tracks are detected.

more similar to the 6-h data than using an identical $V_{\max}$. Using a seemingly unrealistic $V_{\max}$ of 300 km h^{-1} for 1-h data greatly reduces the amount of unrealistic track splitting at a 1-h resolution (Fig. 8c vs 8f). However, using 300 km h^{-1} with 3- or 6-h data leads to frequent unrealistic track continuation (not shown). Essentially, the finer the temporal resolution, the faster the $V_{\max}$ can be to strike a reasonable balance between track continuation and termination.

Using a dynamic $V_{\max}$ brings many aggregated cyclone characteristics into closer alignment when examining all cyclones 1979–2019 (Fig. 9). The number of tracks, average track length, average and maximum cyclone intensity, and the percentage of storms with interactions all become more similar when $V_{\max}$ is made inversely proportional to temporal resolution. The finer resolution data still yields shorter storms that are more intense on average and more likely to be a MCC, but with unrealistic track splitting reduced, the 1-h resolution data yields more cyclones rather than fewer. Also, since $V_{\max}$ is set higher for 1-h resolution tracking, the 1-h resolution results average 5 km h^{-1} faster propagation than the 6-h resolution results.

c. Resolution sensitivity using modified input settings

After modifying the algorithm's input settings to resolve the excess SLP minima and unrealistic track splitting problems that arise for finer spatial and temporal resolutions, respectively,

cyclone detection tracking results still show some sensitivity to resolution. At finer spatial resolutions, more cyclones are detected and a greater percentage of them are MCCs (Figs. 1 and 3). This translates to slightly more cyclone tracks at finer spatial resolution (Fig. 10). Average life span is nearly identical at all spatial resolutions except 200 km, and the 200-km resolution yields significantly larger and weaker storms than the other resolutions.

Storms have systematically shorter track lengths (and therefore slower propagation) at finer spatial resolution, a result of the finer resolution tracks being smoother (Figs. S15 and S16). A greater percentage of storms are MCCs at finer resolution, but cyclone interactions occur at the same relative frequency. All this variation is minor, however, compared to the differences based on temporal resolution, even after adjusting $V_{\max}$ (Fig. 9). Results from 50- and 25-km resolution are especially similar to each other.

The spatial distribution of aggregated cyclone frequency is also more sensitive to temporal resolution than spatial resolution (Fig. 11). Plotting track density with different resolutions can lead to biased interpretations (Zolina and Gulev 2002), so all tracks were interpolated to a 200 km × 200 km grid at 1-h resolution before calculating density statistics. After density calculations, smoothing data to an 800 km × 800 km area removes residual noise.
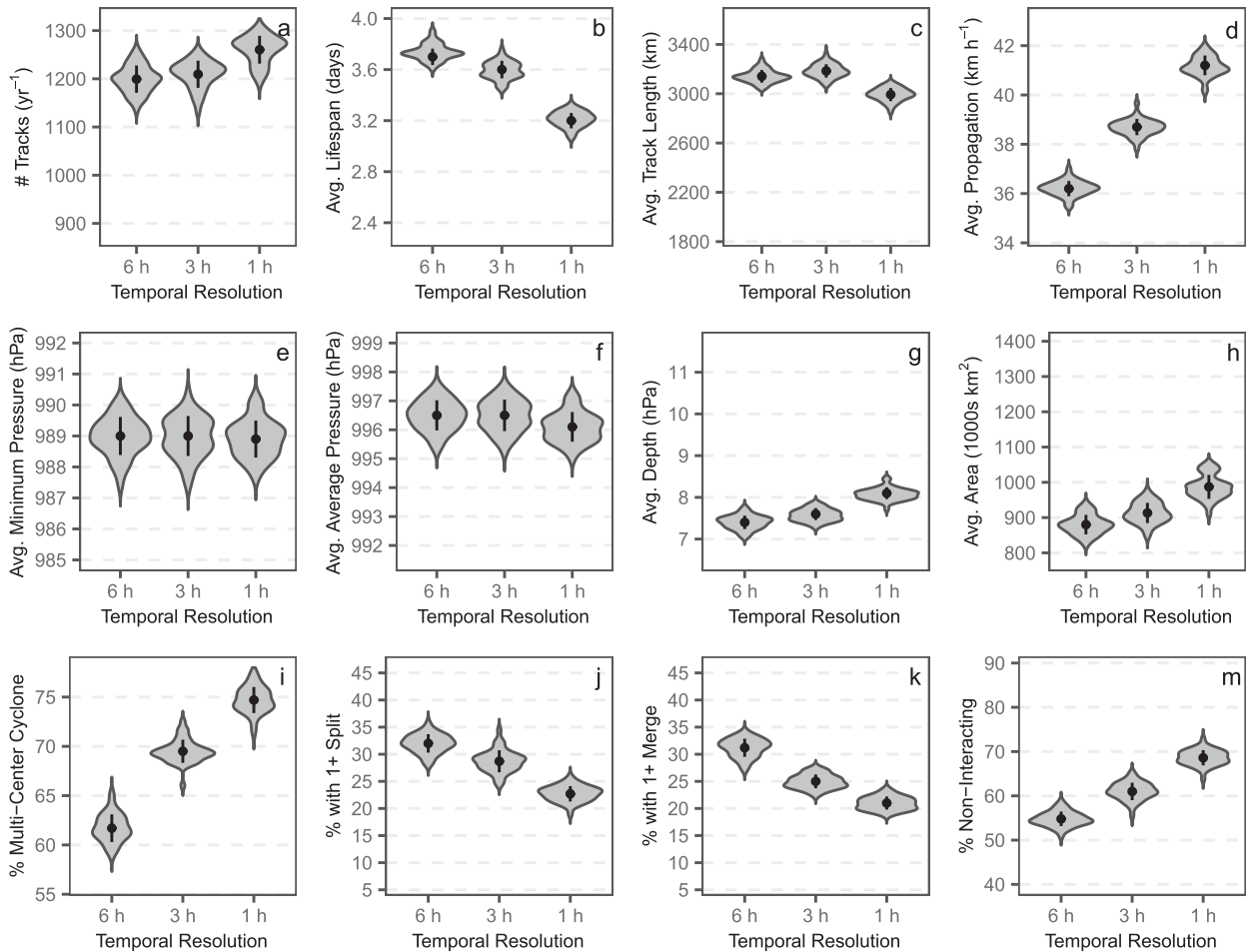
FIG. 9. As in Fig. 5, but with a dynamic maximum propagation speed of 125, 192, and 300 km h^{-1} for 6-, 3-, and 1-h resolutions, respectively. (b)–(d),(g)–(m) All means are significantly different ($p < 0.05$). In other panels, no significant difference exists (e) between any mean or (a),(f) between 6 and 3 h.

Track density is significantly higher at 100-km resolution than at 200-km resolution throughout most of the Northern Hemisphere, with the lee of the southern Rockies being a notable exception (Figs. 11a–c vs 11d–f). Refining spatial resolution to 50 or 25 km increases track density slightly in the Pacific Ocean around 30°N (Figs. 11e,h,k). This may result from the algorithm detecting smaller tropical systems at finer resolution. However, significant differences are minor between 100 and 50 km, and absent between 50 and 25 km. In other words, if a common search distance is used during SLP minima detection, refining resolution beyond 100 km does not make a notable difference to track density.

The sensitivity to temporal resolution is stronger, and despite the number of tracks being higher at a finer temporal resolution, the track density is generally lower because average track length is lower (Fig. 9). Comparing the 50-km resolution results, the average cell-to-cell difference between 1- and 3-h resolution is 12.9% ($p < 0.01$) for cells with at least 10 tracks per year. By contrast, the difference between 3- and 6-h resolution is only 2.6% ($p < 0.01$). Sensitivity is especially high in Alaska, Manchuria, and Baffin Bay and lower in the North

Pacific and Arctic Oceans. Note that sensitivity to temporal resolution increases dramatically if V_{max} is held at a constant 150 km h^{-1} (Fig. S17).

Finally, different experiments can be compared by matching individual tracks. Following Hodges et al. (2003), we consider two tracks from different experiments a match if 1) at least 60% of the combined cyclone observations are shared and 2) the average distance between the tracks for those shared observation times is no more than 500 km. The higher the percentage of tracks in an experiment that meet these criteria, the more consistent the results between the two experiments. Percentages must be calculated in both directions because 1) the denominators (the total number of tracks in the experiments) can differ and 2) sometimes a single track in one experiment can be matched with two distinct tracks in the other.

Results from track-matching (Table 3) are consistent with track density and total cyclone counts. The percentages in Tables 3a and 3c are all over 75%, and all over 85% for 100-km resolution or finer. This again shows that tracks generated by different spatial resolution inputs are comparable, especially at resolutions of 100 km or finer. However, the percentages in
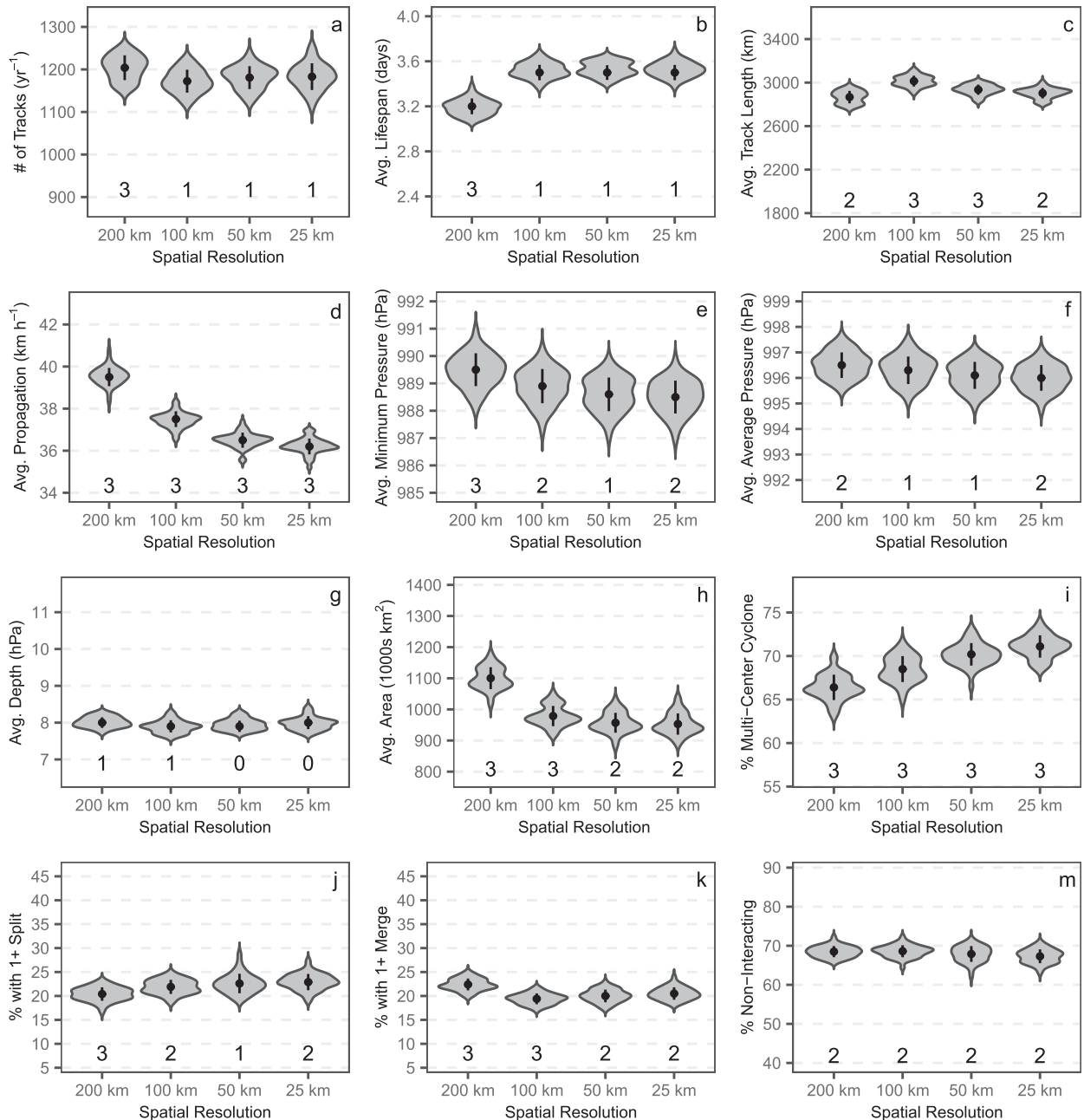
FIG. 10. Violin plots showing the distribution of annual averages of cyclone track statistics for 3-h temporal resolution, $150 \, \text{km h}^{-1}$ maximum propagation, and 200-km search distance. Formatting otherwise follows Figs. 5 and 9. The numbers below each violin indicate how many of the other violins (0–3) have a significantly different mean value using $p < 0.05$.

Tables 3b and 3d range from 51.9% to 86.5%, showing that different temporal resolutions lead to disparate populations of tracks, especially when using a 1-h temporal resolution. Comparing tracks for 6- and 1-h data yield the fewest matches. Higher percentages in Table 3a vs Table 3c and Table 3b vs Table 3d show that using a dynamic V_{max} improves track-matching for different spatial resolutions and different temporal resolutions, respectively. As with other results, Table 3 shows that track-matching is more sensitive to temporal

resolution than spatial resolution, and using a dynamic V_{max} reduces (but does not eliminate) sensitivity to temporal resolution.

4. Discussion

Past studies have concluded that refining spatial resolution when detecting and tracking extratropical cyclones yields significant gains in precision and accuracy of results, primarily
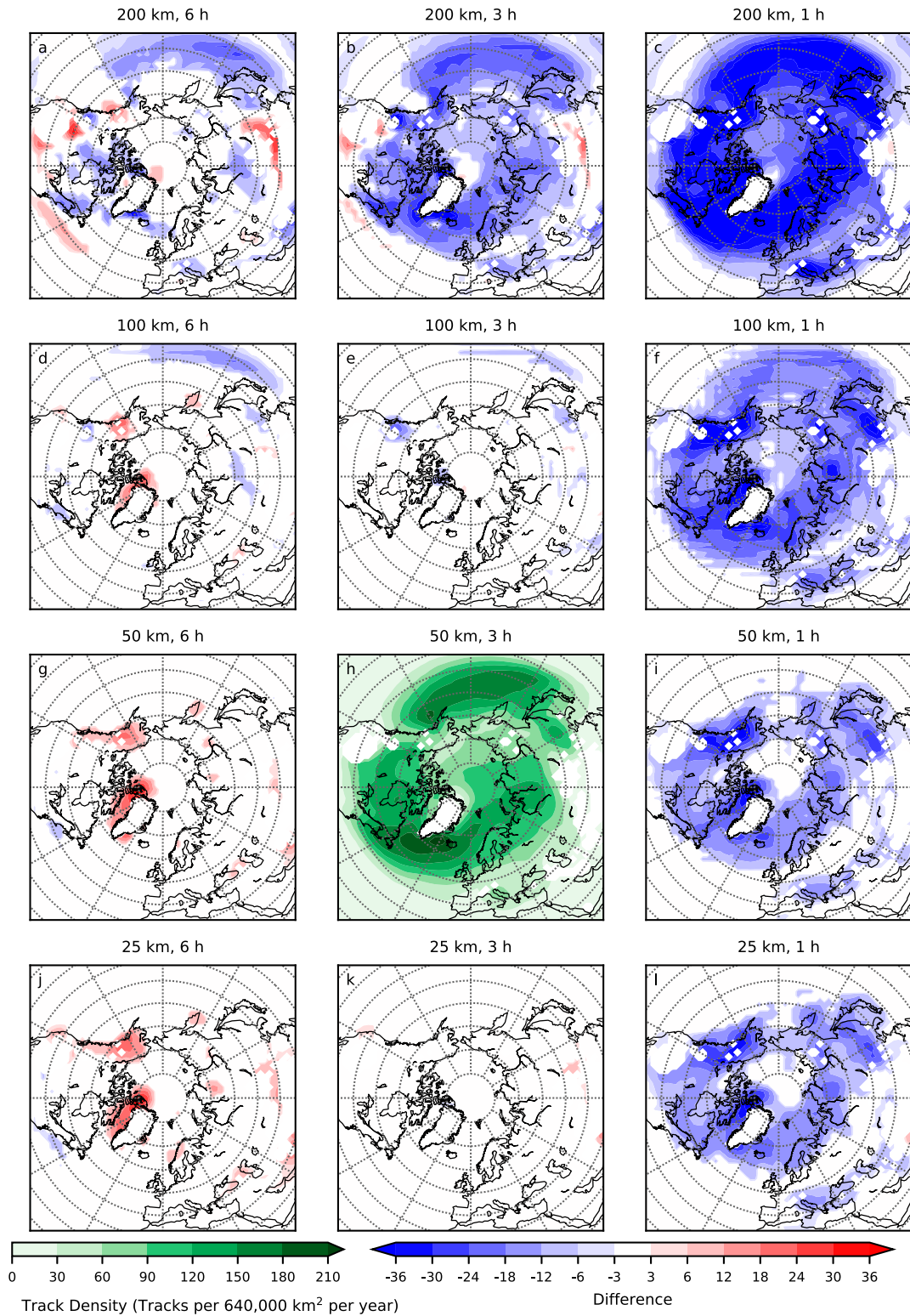
FIG. 11. Difference in average track density (tracks per $640\,000\,km^2$ per year) for the period 1979–2019 using a 200-km search distance and dynamic maximum propagation speed for all combinations of three temporal resolutions (columns) and four spatial resolutions (rows). All differences are relative to 50-km spatial resolution and 3-h temporal resolution in (h). Only significant differences ($p < 0.05$; Welch's t test) are plotted.

TABLE 3. Percentage of cyclone tracks per experiment that can be directly matched to a track in another experiment (sharing at least 60% of combined observation times and averaging no more than 500 km separation). Experiments are grouped by whether temporal resolution or spatial resolution is held constant (left vs right) and whether V_{max} is dynamic or constant (top vs bottom). All experiments use a search distance of 200 km.

a. Temporal resolution = 3 h and max propagation speed = dynamic (192 km h^{-1})				b. Spatial resolution = 50 km and max propagation speed = dynamic			
	200 km	100 km	50 km	25 km		6 h and 125 km h^{-1}	3 h and 192 km h^{-1}	1 h and 300 km h^{-1}
200 km	—	77.7	77.5	76.2	6 h and 125 km h^{-1}	—	86.5	79.2
100 km	78.3	—	87.9	87.4	3 h and 192 km h^{-1}	85.3	—	84.9
50 km	76.8	86.4	—	91.6	1 h and 300 km h^{-1}	75.0	81.5	—
25 km	77.1	85.8	91.4	—				

c. Temporal resolution = 3 h and max propagation speed = 150 km h^{-1}				d. Spatial resolution = 50 km max propagation speed = 150 km h^{-1}			
	200 km	100 km	50 km	25 km		6 h	3 h	1 h
200 km	—	75.6	75.3	75.1	6 h	—	79.3	51.9
100 km	76.7	—	86.8	86.5	3 h	83.1	—	61.4
50 km	75.8	86.2	—	91.3	1 h	58.5	66.6	—
25 km	75.4	85.8	91.2	—				

because coarser resolution data fails to capture weaker and open systems (e.g., Blender and Schubert 2000; Pinto et al. 2005; Jung et al. 2006). These findings are based on detection and tracking algorithms that were first developed for datasets with resolutions ranging from 1° to 3° and 6 to 24 h (e.g., Murray and Simmonds 1991; Sinclair 1994; Serreze 1995; Blender et al. 1997). Subsequent studies have sometimes employed modifications to these algorithms, but many core input settings have gone unchanged, such as using a common number of nearest neighbors to detect SLP (or geopotential height) minima for all spatial resolutions [e.g., Blender et al. (1997) vs Raible et al. (2018) or Bardin and Polansky (2005) vs Zahn et al. (2018)].

Most past work has been limited spatial resolutions no finer than 100 km (e.g., Blender and Schubert 2000; Pinto et al. 2005). Problems with refining spatial resolutions beyond ~100 km/1° were noted by Rohrer et al. (2020), who found that when refining spatial resolution to the native ERA5 grid (T639), one cyclone and tracking algorithm (Blender et al. 1997) identified more cyclones, as expected, but the storms had shorter life spans on average. The other algorithm (Wernli and Schwierz 2006) identified fewer cyclones at a finer resolution, contrary to expectations, but was more consistent in depicting other cyclone characteristics. Both algorithms use eight nearest neighbors when detecting SLP minima, but the algorithm based on Wernli and Schwierz (2006) merges any SLP minima within 1000 km of each other, making it less sensitive to spatial resolution.

We found a similar result to the Blender et al. (1997) algorithm: many more cyclone centers were detected at finer resolution for any individual observation time. However, the additional cyclones found when using 50- or 25-km resolution instead of 100-km resolution were spurious, resulting from the unrealistic breakup of MCCs (Figs. 1–4). Using the 24 nearest neighbors for SLP minima detection at 100-km resolution effectively means all cyclone centers must be over 200 km apart,

but at 25-km resolution, the limit is only 50 km apart (Fig. S2). Any algorithm that uses SLP (or geopotential height) minima as the basis for detection may be sensitive to spatial resolution unless 1) a similar distance-based detection is employed or 2) the input fields are smoothed prior to detection (e.g., Hoskins and Hodges 2002; Côté et al. 2015). We addressed this unrealistic effect by adjusting the number of nearest neighbors based on spatial resolution to match a common distance rather than a common number of neighboring cells. Compared to Wernli and Schwierz (2006), this method allows cyclone centers to be within 200–300 km of each other (as opposed to 1000 km), and the ability to detect MCCs and secondary cyclogenesis is maintained.

Given the problems associated with cyclone detection and tracking at finer resolutions (summarized in Table 4 and Table 5 for spatial and temporal resolution, respectively) we question whether using the latest generation of reanalysis products at their finest-possible resolution is always worthwhile. Synoptic-scale cyclones have radii of 100s to 1000s of km, so refining spatial resolution adds more noise, not just more complexity (Rohrer et al. 2020). Additionally, once this noise is eliminated, overall statistics like track density or average cyclone intensity are comparable for 100-, 50-, and 25-km resolutions (Figs. 10 and 11; Table 4). Note, though, that 200- and 100-km results were still notably different from each other even after standardizing the search distance (Figs. 10 and 11). Since finer spatial resolution also increases computation time, a 100-km resolution is likely sufficient for research questions focused only on aggregated statistics of synoptic-scale cyclone activity on continental or global scales.

Conversely, using finer spatial resolution will provide more precise storm locations, which may be desirable if examining cyclogenesis and cyclolysis or comparing storm tracks to local scales (e.g., a particular weather station). The size and shape of storms can also be more precisely identified. For example, rain-on-snow events in the Arctic, increasingly recognized as having

TABLE 4. Summary of the impact on cyclone detection when changing from coarser to finer spatial resolution (from 100 to 25 km at 3 h). "No change" means the difference is not significant ($p \geq 0.05$).

	Finer spatial resolution	
	Detection based on 24 nearest neighbors	Detection based on 200-km search distance (variable number of neighbors)
Center location	More precise	More precise
Storm frequency (per SLP field)	Many more storms (17.6 → 34.7)	Slightly more storms (17.6 → 18.4)
Cyclone size	Less total cyclone area (smaller storms) (16.3 → 9.6 million km^2 total)	No change
MCC detection (Centers: Cyclones)	Higher percentage of storms identified as MCCs (1.13 → 1.22); more complex MCCs unrealistically broken up	Slightly higher percentage of storms identified as MCCs (1.13 → 1.14)
Computation time	Time quadruples if refined to half resolution	Time quadruples if refined to half resolution

large impacts on herbivore grazing, can be quite localized (Pall et al. 2019; Crawford et al. 2020). Studying subsynoptic-scale and mesoscale processes associated with synoptic-scale storms also requires a finer resolution, as Hewson and Neu (2015) describe for damaging wind gusts. Refining the temporal resolution also provides higher precision in location, as well as more information about storm growth and decay. If interested in explosive cyclogenesis (e.g., Reale et al. 2019) or the duration of storm passage over a fixed location, for example, a finer temporal resolution may have value. Finer resolution also enhances our ability to use such algorithms to identify storm interactions (e.g., splitting and merging of cyclones).

The most appropriate $V_{\max}$ for cyclone tracking is uncertain. Blender et al. (1997) use 80 km h^{-1}; other algorithms go as high as 250 km h^{-1} (Rudeva et al. 2014). Based in part on concerns raised by Neu et al. (2013) about setting $V_{\max}$ too low, Crawford and Serreze (2016) settled on 150 km h^{-1}. Although

Rudeva et al. (2014) found only minor impacts on overall cyclone characteristics from splitting at points of fast propagation, further study of this setting may be necessary because they used a 6-h resolution. Using 1-h resolution data with the current algorithm led to substantial differences in not only the number of tracks, but also average track length, cyclone size, and cyclone intensity (Fig. 5; Table 5). This result likely has broad relevance since maximum propagation speed or distance is a common aspect of many algorithms (e.g., Hodges 1994; Blender et al. 1997; Trigo 2005).

Using spatial resolution fine enough that tracks can propagate across multiple grid cells per time interval lessens this problem. A more effective way to reduce unrealistic splitting at a 1-h temporal resolution is to use a faster $V_{\max}$. However, sensitivity to temporal resolution remains (Figs. 9 and 11; Table 5). The differences in track counts and track density are smaller than the differences between different detection and

TABLE 5. Summary of impact on cyclone tracking when changing from coarser to finer spatial (100–25 km at 3 h) or temporal (from 6 to 1 h at 50 km) resolution. "No change" means the difference is not significant ($p \geq 0.05$).

	Finer spatial resolution (Independent of $V_{\max}$)	Finer temporal resolution	
		$V_{\max} = 150$ km h^{-1}	Dynamic $V_{\max}$
Shape of track	Smoother	Smoother	Smoother
Recorded characteristics	More precise	More precise	More precise
Track frequency	No change	Fewer tracks (1237 → 1082 yr^{-1})	Slightly more tracks (1199 → 1260 yr^{-1})
Storm life span	No change	Much shorter (3.7 → 2.7 days)	Shorter (3.7 → 3.2 days)
Track length	Slightly shorter (3014 → 2903 km)	Much shorter (3359 → 2179 km)	Slightly shorter (3141 → 2993 km)
Storm depth	No change	Much deeper (7.1 → 9.9 hPa)	Deeper (7.4 → 8.1 hPa)
Storm interactions	Slightly more interactions (31.4% → 32.7%)	Many fewer interactions (56.2% → 19.1%)	Fewer interactions (55.2% → 31.4%)
Genesis/lysis location	More precise	More precise but overestimated in areas with high track density	More precise but underestimated in areas with high track density
Overall comments for finer resolution	Differences around complex topography and at 30°N in west Pacific	Unrealistic track division more likely; short/weak storms fall below minimum life span (24 h)	Unrealistic track continuation more likely; excessively fast propagation possible
Track matching between resolutions	85%–90%	50%–60%	75%–80%
Computation time	Time doubles if refining resolution by half	Time doubles if refining resolution by half	Time doubles if refining resolution by half

tracking algorithms [cf. to Neu et al. (2013) or Vessey et al. (2020)], but they are significant. The results for 1-h resolution and $V_{max} = 150\,\mathrm{km\,h}^{-1}$ are clearly unrealistic (Figs. 6c,f), proving that a common V_{max} for all temporal resolutions can be problematic, but comparisons to manual tracking would be needed to determine the optimal settings.

The results presented here are derived from one dataset and one detection and tracking algorithm. As suggested by Rohrer et al. (2020), different algorithms will have different sensitivities to changing the input data resolution, and some are more flexible than others. Switching to a common search distance instead of a common number of nearest neighbors would be relevant for the many algorithms originally designed with a standard of eight nearest neighbors (a 3×3 kernel) when detecting minima (e.g., Blender et al. 1997; Hanley and Caballero 2012; Akperov et al. 2015). Exceptions include algorithms that smooth the input data before detection (e.g., Hoskins and Hodges 2002) or enforce a minimum distance between cyclone centers (e.g., Zhang et al. 2004). Also note that the original data resolution for climate models or reanalyses also impacts results even if all datasets are reprojected to the same grid (Hodges et al. 2011; Rohrer et al. 2018).

The Crawford and Serreze (2016) algorithm used here is one of a few algorithms that explicitly detects MCCs [see also Inatsu (2009); Kew et al. (2010); and Hanley and Caballero (2012)]. However, the same sensitivity to spatial and temporal resolution is found if the MCC functionality of the algorithm is turned off (Fig. 1b, Figs. S18–S22). Therefore, these results are likely relevant to any algorithm that tracks cyclones as point features (e.g., Blender et al. 1997; Lionello et al. 2002; Wang et al. 2006), especially those enforcing a V_{max} at or below $150\,\mathrm{km\,h}^{-1}$. However, similar experiments with other algorithms would be needed to verify this conclusion.

5. Conclusions

In several studies examining the sensitivity of cyclone detection and tracking to input fields, using finer spatial and temporal resolution has been described as improving results because it better captures the whole range of extratropical cyclones (e.g., Blender and Schubert 2000; Pinto et al. 2005; Jung et al. 2006). However, we show that refining spatial and temporal resolutions beyond 100 km and 3 h, respectively, does not necessarily lead to more accurate detection and tracking. After controlling for the input data source (ERA5) and the detection and tracking algorithm, two key problems were discovered:

1) Using a constant number of neighboring grid cells for determining SLP minima leads to the breakup of complex MCCs at finer spatial resolution. This problem is especially apparent around areas of complex topography (e.g., Alaska and Greenland).
2) Using a constant V_{max} for tracking cyclones leads to unrealistic splitting of tracks at 1-h temporal resolution. This problem is especially apparent for fast-moving systems and is worse with coarser spatial resolution.

Our main findings when addressing these problems are:

1) If a common search distance is used to identify nearest neighbors during detection of SLP minima (instead of a common number of neighbors), MCCs are preserved at finer resolution. Moreover, cyclone frequency and other characteristics are comparable for 100-, 50-, and 25-km resolutions.
2) Since 200-km resolution data fails to capture weaker synoptic-scale systems, 100-km resolution is recommended for broadscale studies. Finer spatial resolution may be required to provide greater precision in other work.
3) Unrealistic splitting of tracks with 1-h resolution data can be mitigated by using a faster V_{max}, but even $V_{max} = 300\,\mathrm{km\,h}^{-1}$ is insufficient to eliminate differences between results from 1-h resolution and coarser temporal resolutions.

Additionally, provided a common search distance is used for detecting minima/maxima instead of a common number of nearest neighbors:

4) Careful consideration of temporal resolution and V_{max} is more important than spatial resolution to cyclone tracking.
5) Any spatial resolution at 100 km or finer combined with 6- or 3-h temporal resolution yields comparable results with varying levels of precision.

These results have two broader implications. First, when comparing multiple datasets, using a common temporal resolution and common detection and tracking method(s) is essential. Comparing historical runs from a climate model to atmospheric reanalyses for bias assessment, for example, may be impeded if resolutions are mismatched. Second, the input settings for a cyclone detection and tracking algorithm should always be reevaluated whenever applying it to data with a new resolution. Previous settings used for coarser resolutions, especially the number of neighbors used during SLP minima detection and the V_{max} used during tracking, may no longer be ideal for high-resolution datasets like ERA5.

REFERENCES

Akperov, M., I. Mokhov, A. Rinke, K. Dethloff, and H. Matthes, 2015: Cyclones and their possible changes in the Arctic by the end of the twenty first century from regional climate model simulations. *Theor. Appl. Climatol.*, **122**, 85–96, https://doi.org/10.1007/s00704-014-1272-2.

——, and Coauthors, 2019: Future projections of cyclone activity in the Arctic for the 21st century from regional climate models (Arctic-CORDEX). *Global Planet. Change*, **182**, 103005, https://doi.org/10.1016/j.gloplacha.2019.103005.

Allen, J. T., A. B. Pezza, and M. T. Black, 2010: Explosive cyclogenesis: A global climatology comparing multiple reanalyses. *J. Climate*, **23**, 6468–6484, https://doi.org/10.1175/2010JCLI3437.1.

Bardin, M. Y., and A. B. Polansky, 2005: North Atlantic oscillation and synoptic variability in the European-Atlantic region in winter. *Izv. Atmos. Oceanic Phys.*, **41**, 127–136.

Blender, R., and M. Schubert, 2000: Cyclone tracking in different spatial and temporal resolutions. *Mon. Wea. Rev.*, **128**, 377–384, https://doi.org/10.1175/1520-0493(2000)128<0377:CTIDSA>2.0.CO;2.

——, K. Fraedrich, and F. Lunkeit, 1997: Identification of cyclone-track regimes in the North Atlantic. *Quart. J. Roy. Meteor. Soc.*, **123**, 727–741, https://doi.org/10.1002/qj.49712353910.

Brodzik, M. J., B. Billingsley, T. Haran, B. Raup, and M. H. Savoie, 2012: EASE-Grid 2.0: Incremental but significant improvements for Earth-gridded data sets. *ISPRS Int. J. Geoinfo.*, **1**, 32–45, https://doi.org/10.3390/ijgi1010032.

Copernicus Climate Change Service, (C3S), 2017: ERA5: Fifth generation of ECMWF atmospheric reanalyses of the global climate. Copernicus Climate Change Service Climate Data Store (CDS), accessed 20 May 2020, https://cds.climate.copernicus.eu/cdsapp#!/home.

Côté, H., K. M. Grise, S.-W. Son, R. de Elía, and A. Frigon, 2015: Challenges of tracking extratropical cyclones in regional climate models. *Climate Dyn.*, **44**, 3101–3109, https://doi.org/10.1007/s00382-014-2327-x.

Crawford, A. D., and M. C. Serreze, 2016: Does the summer Arctic frontal zone influence Arctic Ocean cyclone activity? *J. Climate*, **29**, 4977–4993, https://doi.org/10.1175/JCLI-D-15-0755.1.

——, and ——, 2017: Projected changes in the Arctic frontal zone and summer Arctic cyclone activity in the CESM large ensemble. *J. Climate*, **30**, 9847–9869, https://doi.org/10.1175/JCLI-D-17-0296.1.

——, K. E. Alley, A. M. Cooke, and M. C. Serreze, 2020: Synoptic climatology of rain-on-snow events in Alaska. *Mon. Wea. Rev.*, **148**, 1275–1295, https://doi.org/10.1175/MWR-D-19-0311.1.

Day, J. J., M. M. Holland, and K. I. Hodges, 2017: Seasonal differences in the response of Arctic cyclones to climate change in CESM1. *Climate Dyn.*, **50**, 3885–3903, https://doi.org/10.1007/s00382-017-3767-x.

Di Luca, A., J. P. Evans, A. Pepler, L. Alexander, and D. Argüeso, 2015: Resolution sensitivity of cyclone climatology over eastern Australia using six reanalysis products. *J. Climate*, **28**, 9530–9549, https://doi.org/10.1175/JCLI-D-14-00645.1.

Finnis, J., M. M. Holland, and M. C. Serreze, 2007: Response of Northern Hemisphere extratropical cyclone activity and associated precipitation to climate change, as represented by the Community Climate System Model. *J. Geophys. Res.*, **112**, G04S42, https://doi.org/10.1029/2006JG000286.

Hanley, J., and R. Caballero, 2012: Objective identification and tracking of multicentre cyclones in the ERA-Interim reanalysis dataset. *Quart. J. Roy. Meteor. Soc.*, **138**, 612–625, https://doi.org/10.1002/qj.948.

Hell, M. C., S. T. Gille, B. D. Cornuelle, A. J. Miller, P. D. Bromirski, and A. D. Crawford, 2020: Estimating Southern Ocean storm positions with seismic observations. *J. Geophys. Res. Oceans*, **125**, e2019JC015898, https://doi.org/10.1029/2019JC015898.

Hersbach, H., and Coauthors, 2018: ERA5 hourly data on pressure levels from 1979 to present. Copernicus Climate Change Service (C3S) Climate Data Store (CDS), accessed 10 May 2020, https://doi.org/10.24381/cds.bd0915c6.

——, and Coauthors, 2020: The ERA5 global reanalysis. *Quart. J. Roy. Meteor. Soc.*, **146**, 1999–2049, https://doi.org/10.1002/qj.3803.

Hewson, T. D., and U. Neu, 2015: Cyclones, windstorms and the IMILAST project. *Tellus*, **67A**, 27128, https://doi.org/10.3402/tellusa.v67.27128.

Hodges, K. I., 1994: A general method for tracking analysis and its application to meteorological data. *Mon. Wea. Rev.*, **122**, 2573–2586, https://doi.org/10.1175/1520-0493(1994)122<2573:AGMFTA>2.0.CO;2.

——, B. J. Hoskins, J. Boyle, and C. Thorncroft, 2003: A comparison of recent reanalysis datasets using objective feature tracking: Storm tracks and tropical easterly waves. *Mon. Wea. Rev.*, **131**, 2012–2037, https://doi.org/10.1175/1520-0493(2003)131<2012:ACORRD>2.0.CO;2.

——, R. W. Lee, and L. Bengtsson, 2011: A comparison of extratropical cyclones in recent reanalyses ERA-Interim, NASA MERRA, NCEP CFSR, and JRA-25. *J. Climate*, **24**, 4888–4906, https://doi.org/10.1175/2011JCLI4097.1.

Hoskins, B. J., and K. I. Hodges, 2002: New perspectives on the Northern Hemisphere winter storm tracks. *J. Atmos. Sci.*, **59**, 1041–1061, https://doi.org/10.1175/1520-0469(2002)059<1041:NPOTNH>2.0.CO;2.

Inatsu, M., 2009: The neighbor enclosed area tracking algorithm for extratropical wintertime cyclones. *Atmos. Sci. Lett.*, **10**, 267–272, https://doi.org/10.1002/asl.238.

Jung, T., S. K. Gulev, and I. Rudeva, 2006: Sensitivity of extratropical cyclone characteristics to horizontal resolution in the ECMWF model. *Quart. J. Roy. Meteor. Soc.*, **132**, 1839–1857, https://doi.org/10.1256/qj.05.212.

Kew, S. F., M. Sprenger, and H. C. Davies, 2010: Potential vorticity anomalies of the lowermost stratosphere: A 10-yr winter climatology. *Mon. Wea. Rev.*, **138**, 1234–1249, https://doi.org/10.1175/2009MWR3193.1.

Koyama, T., J. Stroeve, J. J. Cassano, and A. D. Crawford, 2017: Sea ice loss and Arctic cyclone activity from 1979 to 2014. *J. Climate*, **30**, 4735–4754, https://doi.org/10.1175/JCLI-D-16-0542.1.

Lionello, P., F. Dalan, and E. Elvini, 2002: Cyclones in the Mediterranean region: The present and the doubled CO_2 climate scenarios. *Climate Res.*, **22**, 147–159, https://doi.org/10.3354/cr022147.

Murray, R. J., and I. Simmonds, 1991: A numerical scheme for tracking cyclone centres from digital data. *Aust. Meteor. Mag.*, **39**, 155–166.

Neu, U., and Coauthors, 2013: IMILAST: A community effort to intercompare extratropical cyclone detection and tracking algorithms. *Bull. Amer. Meteor. Soc.*, **94**, 529–547, https://doi.org/10.1175/BAMS-D-11-00154.1.

NOAA/National Geophysical Data Center, 2009: ETOPO1 1 Arc-Minute Global Relief Model. NOAA/National Centers for Environmental Information, accessed 18 January 2016, https://doi.org/10.7289/V5C8276M.

Pall, P., L. M. Tallaksen, and F. Stordal, 2019: A climatology of rain-on-snow events for Norway. *J. Climate*, **32**, 6995–7016, https://doi.org/10.1175/JCLI-D-18-0529.1.

Papritz, L., S. Pfahl, I. Rudeva, I. Simmonds, H. Sodemann, and H. Wernli, 2014: The role of extratropical cyclones and fronts for Southern Ocean freshwater fluxes. *J. Climate*, **27**, 6205–6224, https://doi.org/10.1175/JCLI-D-13-00409.1.

Pinto, J. G., T. Spangehl, U. Ulbrich, and P. Speth, 2005: Sensitivities of a cyclone detection and tracking algorithm: Individual tracks and climatology. *Meteor. Z.*, **14**, 823–838, https://doi.org/10.1127/0941-2948/2005/0068.

——, S. Ulbrich, T. Economou, D. B. Stephenson, M. K. Karremann, and L. C. Shaffrey, 2016: Robustness of serial clustering of extratropical cyclones to the choice of tracking method. *Tellus*, **68A**, 32 204, https://doi.org/10.3402/tellusa.v68.32204.

Rae, J. G. L., A. D. Todd, E. W. Blockley, and J. K. Ridley, 2017: How much should we believe correlations between Arctic cyclones and sea ice extent? *Cryosphere*, **11**, 3023–3034, https://doi.org/10.5194/tc-11-3023-2017.

Raible, C. C., P. M. Della-Marta, C. Schwierz, H. Wernli, and R. Blender, 2008: Northern Hemisphere extratropical cyclones: A comparison of detection and tracking methods and different reanalyses. *Mon. Wea. Rev.*, **136**, 880–897, https://doi.org/10.1175/2007MWR2143.1.

——, M. Messmer, F. Lehner, T. F. Stocker, and R. Blender, 2018: Extratropical cyclone statistics during the last millennium and the 21st century. *Climate Past*, **14**, 1499–1514, https://doi.org/10.5194/cp-14-1499-2018.

Reale, M., M. L. R. Liberato, P. Lionello, J. G. Pinto, S. Salon, and S. Ulbrich, 2019: A global climatology of explosive cyclones using a multi-tracking approach. *Tellus*, **71A**, 1611340, https://doi.org/10.1080/16000870.2019.1611340.

Rohrer, M., S. Brönnimann, O. Martius, C. C. Raible, M. Wild, and G. P. Compo, 2018: Representation of extratropical cyclones, blocking anticyclones, and Alpine circulation types in multiple reanalyses and model simulations. *J. Climate*, **31**, 3009–3031, https://doi.org/10.1175/JCLI-D-17-0350.1.

——, O. Martius, C. C. Raible, and S. Brönnimann, 2020: Sensitivity of blocks and cyclones in ERA5 to spatial resolution and definition. *Geophys. Res. Lett.*, **47**, e2019GL085582, https://doi.org/10.1029/2019GL085582.

Rudeva, I., and S. K. Gulev, 2007: Climatology of cyclone size characteristics and their changes during the cyclone life cycle. *Mon. Wea. Rev.*, **135**, 2568–2587, https://doi.org/10.1175/MWR3420.1.

——, ——, I. Simmonds, and N. Tilinina, 2014: The sensitivity of characteristics of cyclone activity to identification procedures in tracking algorithms. *Tellus*, **66A**, 24961, https://doi.org/10.3402/tellusa.v66.24961.

Schreiber, E. A. P., and M. C. Serreze, 2020: Impacts of synoptic-scale cyclones on Arctic sea-ice concentration: A systematic analysis. *Ann. Glaciol.*, **61**, 139–153, https://doi.org/10.1017/aog.2020.23.

Serreze, M. C., 1995: Climatological aspects of cyclone development and decay in the Arctic. *Atmos.–Ocean*, **33**, 1–23, https://doi.org/10.1080/07055900.1995.9649522.

Simmonds, I., and I. Rudeva, 2012: The great Arctic cyclone of August 2012. *Geophys. Res. Lett.*, **39**, L23709, https://doi.org/10.1029/2012GL054259.

——, and ——, 2014: A comparison of tracking methods for extreme cyclones in the Arctic basin. *Tellus*, **66A**, 25252, https://doi.org/10.3402/tellusa.v66.25252.

——, C. Burke, and K. Keay, 2008: Arctic climate change as manifest in cyclone behavior. *J. Climate*, **21**, 5777–5796, https://doi.org/10.1175/2008jcli2366.1.

Sinclair, M. R., 1994: An objective cyclone climatology for the Southern Hemisphere. *Mon. Wea. Rev.*, **122**, 2239–2256, https://doi.org/10.1175/1520-0493(1994)122<2239:AOCCFT>2.0.CO;2.

Sprenger, M., and Coauthors, 2017: Global climatologies of Eulerian and Lagrangian flow features based on ERA-Interim. *Bull. Amer. Meteor. Soc.*, **98**, 1739–1748, https://doi.org/10.1175/BAMS-D-15-00299.1.

Stroeve, J. C., M. C. Serreze, A. Barrett, and D. N. Kindig, 2011: Attribution of recent changes in autumn cyclone associated precipitation in the Arctic. *Tellus*, **63**, 653–663, https://doi.org/10.1111/j.1600-0870.2011.00515.x.

Tilinina, N., S. K. Gulev, and D. H. Bromwich, 2014: New view of Arctic cyclone activity from the Arctic system reanalysis. *Geophys. Res. Lett.*, **41**, 1766–1772, https://doi.org/10.1002/2013GL058924.

Trigo, I. F., 2005: Climatology and interannual variability of storm-tracks in the Euro-Atlantic sector: A comparison between ERA-40 and NCEP/NCAR reanalyses. *Climate Dyn.*, **26**, 127–143, https://doi.org/10.1007/s00382-005-0065-9.

Ulbrich, U., J. G. Pinto, H. Kupfer, G. C. Leckebusch, T. Spangehl, and M. Reyers, 2008: Changing Northern Hemisphere storm tracks in an ensemble of IPCC climate change simulations. *J. Climate*, **21**, 1669–1679, https://doi.org/10.1175/2007JCLI1992.1.

Vessey, A. F., K. I. Hodges, L. C. Shaffrey, and J. J. Day, 2020: An inter-comparison of Arctic synoptic scale storms between four global reanalysis datasets. *Climate Dyn.*, **54**, 2777–2795, https://doi.org/10.1007/s00382-020-05142-4.

Wang, X. L., V. R. Swail, and F. W. Zwiers, 2006: Climatology and changes of extratropical cyclone activity: Comparison of ERA-40 with NCEP–NCAR reanalysis for 1958–2001. *J. Climate*, **19**, 3145–3166, https://doi.org/10.1175/JCLI3781.1.

——, Y. Feng, R. Chan, and V. Isaac, 2016: Inter-comparison of extra-tropical cyclone activity in nine reanalysis datasets. *Atmos. Res.*, **181**, 133–153, https://doi.org/10.1016/j.atmosres.2016.06.010.

Wernli, H., and C. Schwierz, 2006: Surface cyclones in the ERA-40 dataset (1958-2001). Part I: Novel identification method and global climatology. *J. Atmos. Sci.*, **63**, 2486–2507, https://doi.org/10.1175/JAS3766.1.

Zahn, M., M. Akperov, A. Rinke, F. Feser, and I. I. Mokhov, 2018: Trends of cyclone characteristics in the Arctic and their patterns from different reanalysis data. *J. Geophys. Res.*, **123**, 2737–2751, https://doi.org/10.1002/2017JD027439.

Zhang, X., J. E. Walsh, J. Zhang, U. S. Bhatt, and M. Ikeda, 2004: Climatology and interannual variability of Arctic cyclone activity: 1948–2002. *J. Climate*, **17**, 2300–2317, https://doi.org/10.1175/1520-0442(2004)017<2300:CAIVOA>2.0.CO;2.

Zolina, O., and S. K. Gulev, 2002: Improving the accuracy of mapping cyclone numbers and frequencies. *Mon. Wea. Rev.*, **130**, 748–759, https://doi.org/10.1175/1520-0493(2002)130<0748:ITAOMC>2.0.CO;2.